^{13}C Relaxation and Dynamics of the Purine Bases in the Iron Responsive Element RNA Hairpin†

Kathleen B. Hall* and Changguo Tang

Department of Biochemistry and Molecular Biophysics, Washington University School of Medicine, St. Louis, Missouri 63110

Received March 6, 1998; Revised Manuscript Received May 8, 1998

ABSTRACT: The iron responsive element (IRE) RNA hairpin contains a conserved six-nucleotide loop. The NMR structure of this loop showed that the positions of four of its bases are not tightly constrained, while the remaining two are hydrogen-bonded [Laing, L. G., and Hall, K. B. (1996) *Biochemistry 35*, 13586]. To investigate the flexibility of the RNA in the loop and in the stem, ^{13}C NMR relaxation methods have been used to describe the dynamics of the purine bases. IRE hairpins containing [^{13}C]guanosine and [^{13}C]adenosine are used in NMR experiments to measure T_1, $T_{1\rho}$, and NOE values of the bases as a function of temperature (20−37 °C). Data are analyzed using the Lipari−Szabo model-free formalism [Lipari, G., and Szabo, A. (1982) *J. Am. Chem. Soc. 104*, 4546] to determine order parameters and time scales of the motion. Results indicate that the purine bases in the stem have order parameters that are independent of temperature, although they show evidence of both fast (6−40 ps) motions and slower motions at 37 °C. The three purines in the loop exhibit increasingly complex motions with long (nanoseconds) correlation times as the temperature increases, suggesting that the loop structure has become disordered.

RNA sequences that participate in intermolecular interactions are usually found in structures that provide access to the bases, such as single-stranded regions, internal and hairpin loops, and deformations of duplex regions. To make contact with a protein or another nucleic acid, these regions of the RNA must be inherently flexible to allow structural adaptations to accommodate the interaction. A description of flexibility will include the time scales of the dynamic motions of the nucleotides and the energetics of the process, and finally the physical picture of the excursions. The dynamics of a RNA sequence will be as important as its structural context if we are to understand how these sequences become accessible to other components of the cell.

The iron responsive element (IRE) RNA hairpin is part of a larger structure located in the 5′ untranslated region of the ferritin mRNA (*1*). It is specifically recognized by the 90 kDa iron responsive protein (IRP), and formation of the IRE−IRP complex blocks mRNA translation (*2*). The IRE loop is part of the recognition site for the IRP; it contains six nucleotides, two of which are hydrogen-bonded across the loop to stabilize the structure (*3*). The sequence, structure, and flexibility of this loop must all be considered important features of its interaction with the IRP regulatory protein.

The structure of the IRE showed that two purine bases on the 5′ side of the loop were stacked although not otherwise constrained; two pyrimidine bases are apparently free to move (see Figure 1). To more quantitatively describe the dynamics of the bases, we have now used ^{13}C NMR relaxation methods to monitor the fast motions of the nucleotides, in the picosecond to nanosecond range, and to look for evidence of slower motions characteristic of conformational exchange (microsecond to millisecond). This work complements two previous studies of RNA hairpins, one using ^{13}C relaxation to study the dynamics of the HIV TAR RNA stem−loop (*4*) and the other a ^{15}N study of the UUCG tetraloop (*5*) that used the ^{15}N−^{1}H imino resonances from hydrogen-bonded bases. In the IRE experiments, the use of the ^{13}C−^{1}H spin pairs allows the observation of bases in all structural contexts, providing a comparison between properties of bases in the loop and those in the stem.

In nucleic acids, the exchangeable imino N−H can describe only the hydrogen-bonded residues; the nonexchangeable C−H systems are more powerful reporters, but in most cases, the relaxation pathways are complicated by C−C homonuclear cross relaxation. Unless site-specific ^{13}C incorporation is used to simplify the spin systems, only the C_8−H_8 of guanosine and adenosine and C_2−H_2 of adenosine are nearly isolated spin pairs, due to the two flanking aromatic nitrogens. These spin systems can be used in heteronuclear relaxation experiments (*6*−*9*); the obvious limitation is that only a fraction of the RNA nucleotides can be sampled, and the comparison of the dynamics of the sugar and the base is not readily made. These ^{13}C relaxation experiments measure the properties of the nucleotide base, which are analogous to the dynamics of amino acid side chains (*10*, *11*).

The Lipari−Szabo formalism (*12*, *13*) is used here to describe the motion of the purine bases in the IRE, and the resulting order parameters are compared as a function of

† This work is supported by the NIH (Grant GM46318 to K.B.H.).
* Corresponding author. Phone: (314) 362-4196. E-mail: hall@bionmr3.wustl.edu.

S0006-2960(98)00528-5 CCC: $15.00
Published on Web 06/11/1998

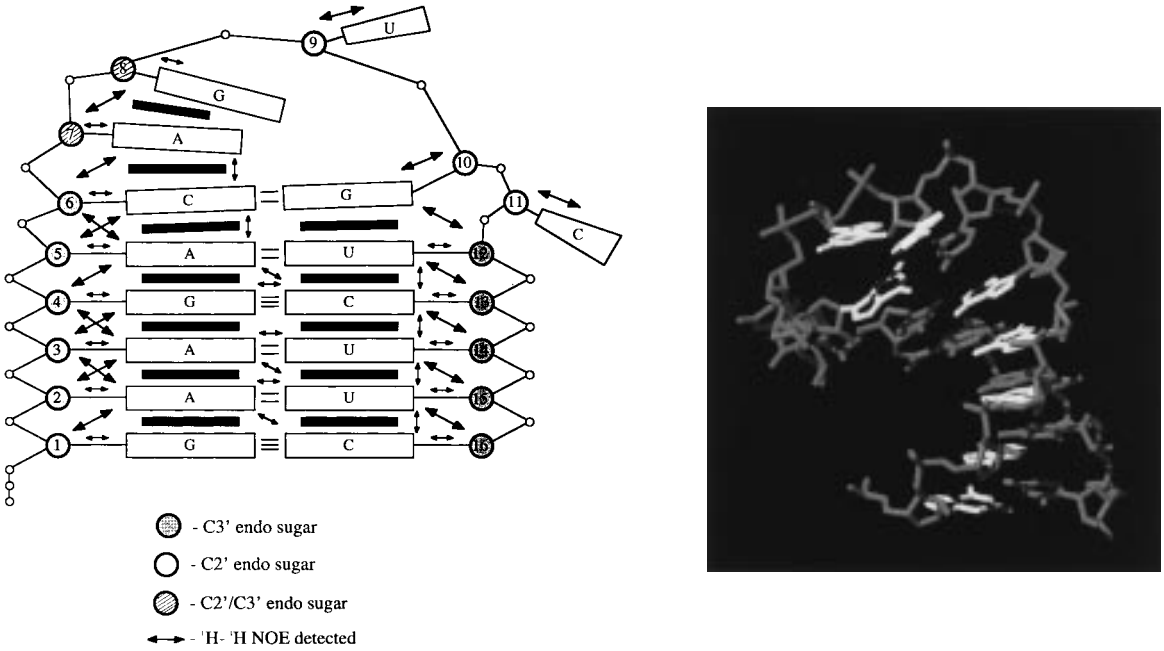

FIGURE 1: Sequence and structure of the IRE hairpin. (Right) The structure shown is one of the family of structures consistent with the NMR data; purine bases are in yellow and pyrimidines, riboses, and phosphates in magenta. (Left) Schematic representation of the structure. The structure was determined at 20 °C in 30 mM NaCl and 10 mM sodium phosphate (pH 6) (*3*).

temperature. Analysis of relaxation data is generally done either through solutions of the spectral densities (*14*, *15*) or with the model-insensitive formalism (*16*); the latter approach has been applied here to the IRE data to allow a comparison with previous NMR studies that describe nucleic acid dynamics in DNA duplexes (*17*, *18*), in DNA hairpins (*19*), and in two RNAs (*4*, *5*). In addition, the time scales and amplitudes of motions could be compared to the results from molecular dynamics simulations of DNAs and RNAs in explicit solvent (*20*−*23*) which are now sufficiently robust to sample time scales described by the NMR data.

While these experiments can describe the time scale of the dynamics, they do not provide a physical picture of the motions, such as base pair opening, relative motions of stacked bases, or coupled sugar and base dynamics. The types of motions accessible to the base might best be compared to motions of aromatic side chains or rotations of methyl groups; several experimental (*11*, *24*) and theoretical (*25*−*28*) treatments have described these systems, and might serve as models for the motions of the base.

MATERIALS AND METHODS

RNA Synthesis. The IRE RNA hairpin was enzymatically synthesized with SP6 RNA polymerase, incorporating [^{13}C]-ATP, [^{13}C]GTP, or both, as described (*3*). Uniformly labeled NTPs were synthesized following the protocol of Nikonowicz et al. (*29*). RNAs were purified by HPLC on a Dionex column and desalted. The final NMR sample contained 2 mM RNA in 30 mM NaCl, 10 mM sodium phosphate (pH 6), and 90% D_2O/10% H_2O.

NMR Experiments. NMR experiments were carried out on either a Varian Unity 500 MHz or Varian Unity 600 MHz spectrometer, with a Nalorac 5 mm triple-resonance probe equipped with *Z*-gradients. In T_1, $T_{1\rho}$, and NOE experiments, pulse sequences of Yamazaki et al. (*30*) were used (without either ^{15}N or ^{13}C′ decoupling). The delays were optimized for the aromatic $J_{HC} = 200$ Hz: $\tau_a = 1.06$ ms, $\tau_b = 2.34$ ms, and $\tau_c = 0.97$ ms. The two-bond C−C scalar couplings are small (≤7 Hz; A. Pardi, personal communcation), and no attempt was made to remove their effect, since they will make no contribution to T_1 or $T_{1\rho}$ relaxation. The constant time interval in experiments was adjusted for resolution in the second dimension (2.5 ms). Carbon was garp-decoupled (*31*) during proton acquisition. Proton pulses were centered at 6.9 ppm with respect to water at 4.8 ppm; carbon pulses for NOE and T_1 experiments were centered at 146.73 ppm and referenced to TMS. For $T_{1\rho}$ experiments with purine $^{13}C_8$ carbons, the 2 kHz spin lock was centered at 142.6 ppm; for $^{13}C_2$ carbons, the carrier was centered at 151.7 ppm. There is effectively no chemical shift dispersion in the carbon spectra, the result being that all carbons are on resonance with respect to the carrier. T_1 delays were 5, 45, 85, 125, 165, 205, 245, 285, 325, 365, 405, 445, 485, 525, 565, and 605 ms; $T_{1\rho}$ delays were 4, 8, 12, 16, ..., and 72 ms. Two-dimensional (2D) experimental data were collected with the hypercomplex method (*32*), with 64 scans per t_1 increment (96 for NOE experiments). Spectral widths for each experiment were adjusted slightly with temperature to accommodate the shifts; peaks were folded in the ^{13}C dimension: 2400 × 1200 Hz (^{1}H × ^{13}C) for NOE experiments, 2100 × 3000 Hz for T_1 experiments, and 3000 × 3000 Hz for $T_{1\rho}$ experiments at 37 °C and 500 MHz. Peak heights in the 2D spectra were calculated using Vnmr software, and the intensity changes with time were fit using Vnmr processing software to the expression $I(t) = I(0)\exp(-t/T_{1,2})$, where $I(t)$ is the intensity at time t or 0. Steady-state NOE values were calculated from the ratios of peak intensity with and without proton saturation. Uncertainties in T_1 and $T_{1\rho}$ data were obtained from the Vnmr fitting program, including duplicate experiments at two delays; errors in NOE experiments were calculated from the standard deviation of two or more measurements. ^{1}H TOCSY and ^{13}C/^{1}H HMQC-

TOCSY experiments were carried out before and after each series of dynamics experiments, as a check on the integrity of the RNA sample.

Data Analysis. Relaxation of the C_8 and C_2 base carbons is dominated by dipolar interaction with the attached nonexchangeable proton and by the chemical shift anisotropy of the carbon nucleus. T_1, T_2, and NOE relaxation parameters are described by (*33*)

$$R_1 = 1/T_1 = (d^2/4)[J(\omega_H - \omega_C) + 3J(\omega_C) + 6J(\omega_H + \omega_C)] + (\omega_C\Delta\sigma/\sqrt{3})^2 J(\omega_C)$$

$$R_2 = 1/T_2 = (d^2/8)[4J(0) + J(\omega_H - \omega_C) + 3J(\omega_C) + 6J(\omega_H) + 6J(\omega_H + \omega_C)] + (\omega_C\Delta\sigma/\sqrt{3})^2/6[4J(0) + 3J(\omega_C)] + R_{ex}$$

$$\mathrm{NOE} = 1 + (d^2/4R_1)(\gamma_C/\gamma_H)[6J(\omega_H + \omega_C) - J(\omega_H - \omega_C)]$$

where $d = \mu_0 h\gamma_C\gamma_H\langle r_{CH}^{-3}\rangle/8\pi^2$, μ_0 is the permeability of free space, h is Planck's constant, γ_C and γ_H are the gyromagnetic ratios of carbon and hydrogen, respectively, ω_H and ω_C are the Larmor frequencies of hydrogen and carbon, respectively, and R_{ex} is an ad hoc parameter that is sometimes invoked to account for observed T_2 relaxation; for the RNA purine bases, $r_{CH} = 1.09$ Å is the aromatic carbon−hydrogen bond length and $\Delta\sigma$ the chemical shift anisotropy. For all purine carbons, $\Delta\sigma = 189$, based on the value of 185 determined for the C_6 of thymine by Williamson and Boxer (*19*); three other values of $\Delta\sigma$ (66, 90, and 130 ppm) were independently minimized with arrays of τ_m, but the residuals of the fits were very large compared to the residuals with a $\Delta\sigma$ of 189. It is likely that the value of $\Delta\sigma$ for purines is not a constant, and these parameters need to be directly measured for future work.

We have used the Lipari−Szabo (*12*, *13*) model-independent formalism to reduce the spectral densities (*16*) where

$$J(\omega) = S^2\tau_m/(1 + \omega^2\tau_m^2) + (1 - S^2)\tau/(1 + \omega^2\tau^2)$$

The order parameter, S^2, describes the spatial distribution of the internal motion of the ^{13}C−^{1}H bond vector, which here will describe the motion of the entire base, since this vector is fixed by the sp^2 geometry of the aromatic carbon. Values for S^2 of 1 describe completely restricted motion, and an S^2 of 0 corresponds to unrestricted motion. τ_m is the overall tumbling time of the molecule, and $1/\tau = 1/\tau_m + 1/\tau_e$, where τ_e is an effective correlation time for local internal motions. This formalism was extended (*34*) for the case where internal motions occurred on two time scales that differed by more than 1 order of magnitude:

$$J(\omega) = S^2\tau_m/(1 + \omega^2\tau_m^2) + (S_f^2 - S^2)\tau/(1 + \omega^2\tau^2)$$

where now the order parameter is the product of two uncorrelated order parameters S_f^2 and S_s^2, which describe fast and slow internal motion, respectively. The correlation time for slow internal motions is included in the expression $1/\tau = 1/\tau_s + 1/\tau_m$.

The Lipari−Szabo formalism accommodates both isotropic and anisotropic overall tumbling, and our analysis software is designed to calculate parameters using either model.

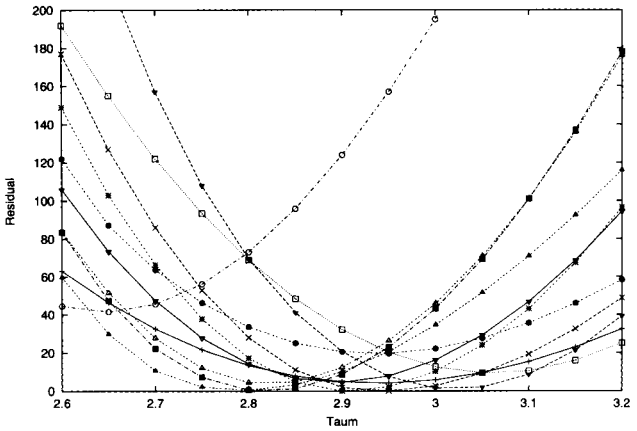

FIGURE 2: χ^2 vs τ_m for each purine base in the IRE at 30 °C, using the simple Lipari−Szabo model of motion. T_1 data at 600 MHz were also used in the minimization.

Dimensions of the IRE hairpin are roughly spherical, since it is 20 Å wide (the width of the A-form duplex) and 20 Å high (approximating the loop as a 3 bp stem and disregarding any deformations that occur when its stacking is disrupted), suggesting that the isotropic model of overall tumbling would be adequate. In fact, a comparison of fits of the data with each model of overall tumbling indicated that the hairpin can be accurately described as an isotropically tumbling system (data not shown), so this simplifying assumption was used for all subsequent analysis.

Determination of τ_m. To determine the optimal τ_m of the hairpin, an array of τ_m values was used as input for a minimization in parameter space using the Lipari−Szabo formalism. For each τ_m in the array, T_1, $T_{1\rho}$, and NOE values of each residue are fit to each model. The program allows values of T_1, $T_{1\rho}$, and NOE from both 500 and 600 MHz experiments to be incorporated into the parameter array; for these experiments, only T_1 values at 30 °C were collected at both frequencies. The residuals χ^2 of the target function

$$\chi^2 = (T_1^{exp} - T_1^{c})^2/\sigma_1^2 + (T_2^{exp} - T_2^{c})^2/\sigma_2^2 + (\mathrm{NOE}^{exp} - \mathrm{NOE}^{c})^2/\sigma_3^2$$

were calculated for each residue using the simple model. The superscript indicates experimental (exp) and calculated (c) values. The standard deviations (σ_i) of the T_1, T_2 ($T_{1\rho}$), and NOE values for each peak are determined from experimental data.

Graphs of χ^2 versus τ_m are displayed for all residues at each temperature; a typical example is shown in Figure 2. The best correlation time (τ_m) for the system is that value that gives the smallest sum of all residuals. This method of determining the rotational correlation time of the RNA differs from the approach taken with protein ^{15}N backbone relaxation parameters, where the T_1/T_2 ratio can be reliably used to estimate τ_m. For the RNA hairpin, there are data from only eight purine bases, which could not be assumed to accurately represent the overall tumbling time of the hairpin. However, a plot of τ_m versus η/T is linear, as expected (data not shown), indicating that the selected overall tumbling time of the molecule was appropriate.

Each minimization consists of a global grid search and a local search. The optimized values of S^2, τ_e, etc., from the global search are used as initial points for a local search using

the full Newton method (*35*) for further minimization of χ^2. Errors in the final parameters are calculated using 1000 Monte Carlo simulations (*35*), based on the optimized parameter set.

Calculation of σ_χ. To express the order parameters in terms of a physical model of the motion, the simple interpretation of Bruschweiler and Wright (*36*) of a weighted Gaussian axial fluctuation (GAF) for a vector on the surface of a cone was used. Applied to the purine bases, the glycosidic bond (χ) is the director axis about which the cone is defined; the C−H vectors describe the cone generated about this central axis. The angles β between the C−H vector and the glycosidic bond $N_9-C_{1'}$ were measured using TURBO (*37*) to give the following: $\beta = 73.5°$ for adenosine C_8−H, $\beta = 77.7°$ for adenosine C_2−H, and $\beta = 72.8°$ for guanosine C_8−H. These β values together with the order parameters from the relaxation analysis were used as input in the expression

$$S^2 = 1 - 3\sin^2\beta\{\cos^2\beta[1 - \exp(-\sigma^2_\chi)] + {}^1/_4\sin^2\beta[1 - \exp(-4\sigma^2_\chi)]\}$$

to solve for σ_χ, the standard deviation about χ. Numerical solutions to the equation were obtained using Maple V; the resulting values of σ_χ in radians were converted to degrees. This model was applied to RNA bases by Akke et al. (*5*), and thus provides a comparison for the IRE results.

RESULTS

The IRE RNA hairpin used in this work contains five base pairs in the stem (two G·C pairs and three A·U pairs) and six nucleotides in the loop. Among the loop nucleotides (6C-7A-8G-9U-10G-11C), 9U and 11C are not constrained by NMR data, and presumably have many conformations accessible (9U in particular). 10G is hydrogen-bonded across the loop to 6C which stabilizes the structure, while 7A and 8G are stacked over each other above 6C. 11C is extruded from the structure, allowing 10G to stack over the loop-closing base pair (5A·12U) (see Figure 1). The two base pairs at the stem terminus (1G·C and 2A·U) adopt several conformations that are stable on the NMR time scale, as demonstrated by the two and sometimes three resonances from the purine H_8 and H_2 protons (*3*; see Figure 3).

In these ^{13}C relaxation experiments, we have analyzed the behavior of the purine $^{13}C_8-^1H$ and $^{13}C_2-^1H$ spin pairs in uniformly labeled [^{13}C]adenosine, [^{13}C]guanosine, and [^{13}C]-adenosine/[^{13}C]guanosine RNAs. These $^{13}C-^1H$ systems of the purine nucleotides are virtually isolated spin pairs; there is no carbon−carbon homonuclear cross relaxation, and the contribution of scalar relaxation of the second kind from the adjacent ^{14}N quadrupolar nuclei is calculated to be negligible (*38*). Thus, the dominant relaxation pathways are dipolar from the covalently attached proton and CSA (chemical shift anisotropy) of the ^{13}C itself, allowing the application of relaxation and dynamics analysis as it has been used for the amide backbone of proteins or the $^{15}N-^1H$ imino of RNA. The use of the nonexchangeable $^{13}C-^1H$ systems for analysis of RNA is critical for comparison of the dynamic properties of the loops, noncanonical structures, and duplex regions, since the imino protons of bases in unstructured regions are typically in fast exchange with solvent.

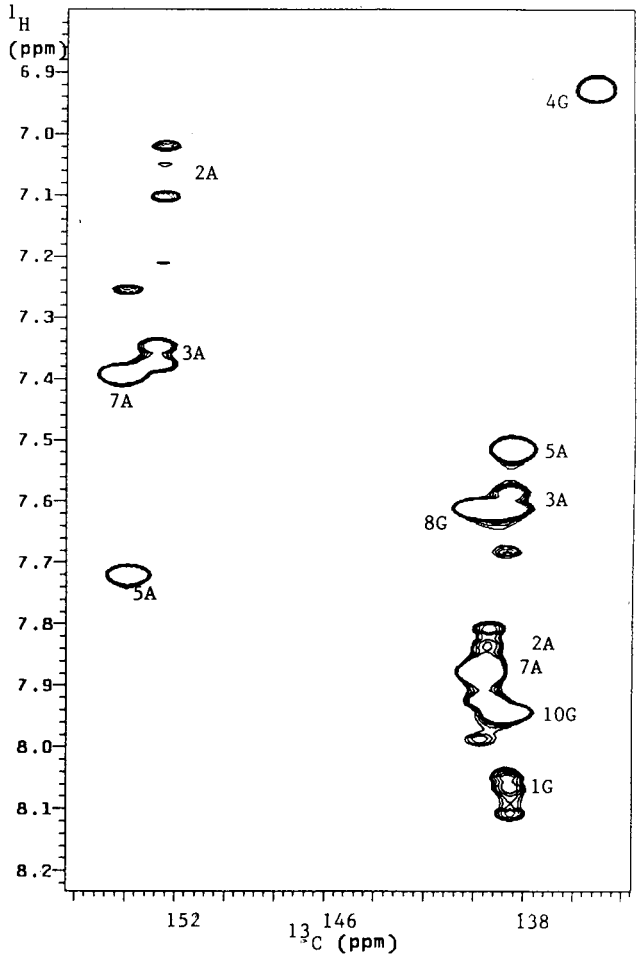

FIGURE 3: 2D $^{13}C/^1H$ HMQC spectrum at 500 MHz of the [^{13}C]-adenosine, [^{13}C]guanosine doubly labeled IRE RNA, showing the aromatic region with assignments. Note that there are several cross-peaks assigned to 1G, 2A C_2, 3A C_2, 2A C_8, and 3A C_8. Measured in 2 mM RNA at 30 °C, 30 mM NaCl, 10 mM sodium phosphate (pH 6), and 2 mM RNA.

Purines in the IRE. This IRE hairpin has eight purine bases, five in the stem and three in the loop. The 2D $^{13}C/^1H$ HMQC spectrum of the RNA is shown in Figure 3; the four adenosine $^{13}C_2$ are centered around 152 ppm, while the guanosine and adenosine $^{13}C_8$ are centered around 136 ppm. The conformational heterogeneity of the first base pair of the stem (1G·C) is seen from the two proton resonances associated with the $^{13}C_8$; the second base pair 2A·U also has several conformations, as observed from the two distinct proton resonances corresponding to $^{13}C_2$, and its $^1H-^{13}C_8$ cross-peak is very broad. In the analysis of the relaxation data, each peak assigned to a carbon−proton pair was processed; as a first approximation, decay curves from these residues were fit and described as they were for the other residues. The measured rate of conformational exchange at these positions, which is on the order of the chemical shift difference ($\Delta\delta$), is between 2.5 and 5.0 ms (400−200 s^{-1}) for 1G·C and 2A·U, determined from the chemical shift differences of the protons. Note that the carbon chemical shift corresponding to several protons assigned to a given $^{13}C-^1H$ system does not change; the conformational heterogeneity is apparent only in the proton dimension.

The data reported here are for a [^{13}C]adenosine/guanosine IRE molecule. Singly labeled RNAs were synthesized and

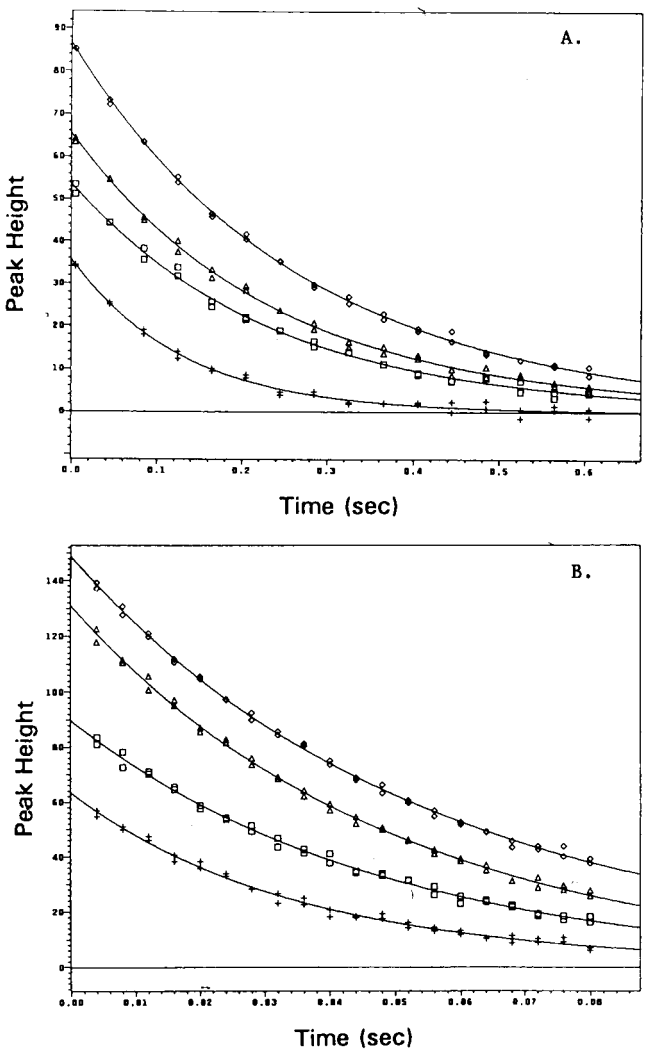

FIGURE 4: T_1 (A) and $T_{1\rho}$ (B) exponential decay curves for the four guanosine $^{13}C_8$ in the IRE at 30 °C and 600 MHz. Duplicate data sets are given as discrete points; the curve is the two-parameter exponential fit.

used in relaxation experiments, but although their structures appeared to be identical on the basis of their ^{1}H and ^{13}C chemical shifts, it was impossible to directly compare their relaxation parameters since the salt concentrations were difficult to reproduce exactly. The flexibility of this RNA hairpin thus appears to be very sensitive to the salt (NaCl) concentration, and probably also to the specific counterion. This is likely to be a common feature of RNA structures, and one that can now be investigated in terms of the effects on nucleotide dynamics.

The T_1 and $T_{1\rho}$ relaxation times for each purine base in the doubly labelled IRE hairpin were calculated from a two-parameter fit of the single-exponential decay curves at 20, 30, and 37 °C. Examples of the data are shown in Figure 4 for the four guanosine $^{13}C_8$ at 30 °C and 600 MHz. Each experiment was carried out in duplicate, and the peak intensities from each experiment are shown, together with the fit to the data. In subsequent experiments, only two time points were done in duplicate. Errors in the relaxation values are calculated from the experimental data, and are typically 1−2%, although errors in the NOE values are larger (5−10%). The values of T_1, $T_{1\rho}$, and the ratio $T_1/T_{1\rho}$ for each purine are given in Figure 5. As the data show, at 20 and 30 °C, there is little variation in relaxation times with the structural context of the purine base; however, at 37 °C, it is apparent that the bases in the loop (7A, 8G, and 10G) have larger $T_{1\rho}$ values than do the purines in the stem (1G, 2A, 3A, 4G, and 5A). However, the values of the NOE ratio (Figure 5) suggest that, even at 20 °C, there is a difference between the dynamics of bases in the loop and those in the stem; 10G (which is hydrogen-bonded to 6C of the loop) appears more like the stem bases at lower temperatures.

Model-Insensitive Analysis. All residues were analyzed using the Lipari−Szabo formalism, with its reduced form of the spectral density. The parameters were fit to the simple model including an order parameter (S^2) and an effective (internal) correlation time for fast motion (τ_e); to the simple model that included a T_2 exchange parameter (R_{ex}); and to the extended form which includes order parameters for shorter and longer time scale motion (S_f^2 and S_s^2, respectively), where $1/\tau = 1/\tau_m + 1/\tau_s$.

The order parameter, S^2, for each position in the purine bases is shown in Figure 6 as a function of temperature for each of the three models. At 20 °C, all models give very uniform values of order parameters throughout the molecule, centered at an S^2 of 0.78. At this temperature, the purines in the loop are not readily distinguishable from those in the stem, which is consistent with the structural data showing that the loop nucleotides are stacked (the structure was solved at 20 °C). At 30 °C, there is some indication that the two previously stacked loop purines (7A and 8G) have lower order parameters; 10G again looks like the bases in the stem. By 37 °C, there is a significant reduction in the order parameter of 7A, 8G, and also 10G, while the stem bases maintain an average S^2 of 0.8.

DISCUSSION

A summary of the parameters that best describe the dynamics of each purine base is given in Tables 1−3. Data are given for those residues that have well-resolved resonances at each temperature. Selection of a model for describing the ^{13}C−^{1}H vector motion is based on the magnitude of the residual (χ^2) as well as physically meaningful values of the associated parameters. Occam's razor was the final criterion in those cases where several models appeared to fit the data. It is disappointing that the errors on the values of R_{ex} and $\tau_{s,e}$ are very large, precluding their utility in quantitative descriptions of the dynamics.

Structure and Dynamics

This IRE hairpin contains a stem in which the terminal base pair exhibits conformational heterogeneity on the NMR time scale, as well as a six-nucleotide loop where two residues are in a hydrogen-bonded pair, two purines are stacked, and two pyrimidines are unconstrained. The variety of nucleotide conformational states in this small RNA hairpin provides the opportunity to measure the dependence of RNA dynamics on different structural contexts.

IRE Stem. All purine bases in the stem of the IRE exhibit very uniform order parameters, independent of the temperature. The average value of S^2 at 20 °C is 0.77, and at 30 and 37 °C, the average value is 0.80. To analyze the terminal 1G purine and the 2A purine, which have two or three H_8 or H_2 resonances, each peak was separately processed,

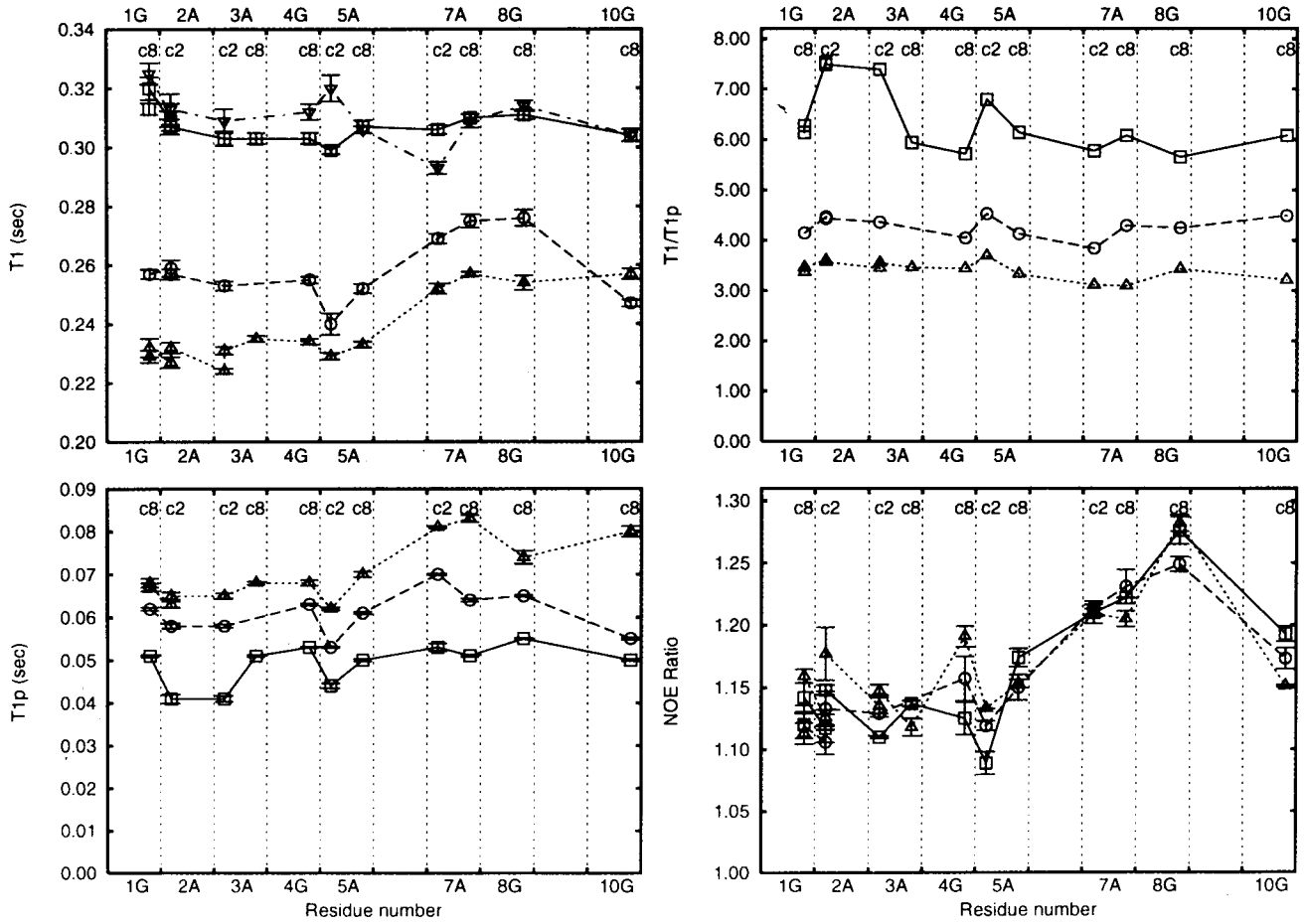

FIGURE 5: Measured T_1 (top left) and $T_{1\rho}$ (bottom left) values for the purines as a function of temperature and the ratio $T_1/T_{1\rho}$ (top right). The T_1 data include experimental data at 600 MHz (▽). Errors were calculated from the fit to the exponential decay. Measured NOE ratios (bottom right) for the purine bases as a function of temperature: (□) 20, (○) 30, and (△) 37 °C. Standard deviations were calculated from experimental values, based on duplicate experiments. Individual $^{13}C-^{1}H$ values are shown, including those with two resonances; connecting lines are for ease of visualization only.

making the simplifying assumption that the time scales of their conformational exchange would not be correlated with the time scales of the ^{13}C dynamics. This assumption appears to be valid, since the model parameters obtained for all purines in the stem are very similar.

Despite the uniformity of their order parameters, the bases in the stem have increasingly more complex motions as the temperature increases. While R_{ex} terms do appear in the fits for the $T_{1\rho}$ data for the bases in the stem at 20 °C, their values are too small to be reliable; at 30 °C, the data from the stem bases are best fit by the simple model with only S^2 and τ_e (with the exception of 5A). At 37 °C, the values of R_{ex} are substantial for both resonances corresponding to 2A C_2 (0.8 ± 0.9 s^{-1}), for one of the 3A C_2 resonances (0.6 ± 0.8 s^{-1}), for 4G (0.4 ± 0.7 s^{-1}), and for 5A C_2 (1.2 ± 1 s^{-1}) which is the loop-closing base pair. The RNA hairpin is intact at 37 °C (its melting temperature in this low salt is about 55 °C), so the increase in the magnitude of the exchange terms is not the result of melting of the stem. The need for the ad hoc addition of the R_{ex} terms may reflect genuine changes in the dynamic behavior of the base, such as if there were more frequent opening of the base pairs or increased mobility of stacked bases. However, the need for R_{ex} terms may reflect a poor fit of the model to the data. It will be critical to verify the interpretation of the R_{ex} terms as an indication of conformational exchange, which can be done by varying the spin lock power in the $T_{1\rho}$ experiment and extracting the exchange contribution (*39*, *40*). In addition, a Brownian dynamics simulation of RNA base pair opening can estimate the correlation times of fluctuations of the base as a function of the rotation angle, as previously done for DNA (*41*); these results may be compared with the NMR analysis.

Other Duplexes. Relaxation data for two other RNA duplexes come from the experiments of King et al. (*4*) using [^{13}C]adenosine in the HIV TAR RNA hairpin and from the ^{15}N experiments of Akke et al. (*5*) for the UUCG tetraloop hairpin. Using the Lipari−Szabo formalism, King et al. calculated the average order parameter for the adenosine bases in the TAR stem which appears to be close to 0.85. The order parameters obtained for the $^{13}C_2$ and $^{13}C_8$ of each adenosine base in the TAR hairpin were not identical, but there was no consistent pattern of variation between the two sites; similar results are observed for the adenosines in the IRE stem. For the UUCG tetraloop at 0 °C, analysis of the ^{15}N imino relaxation of the uridine and guanosine bases resulted in order parameters from 0.74 for the fraying terminal G·C pair to 0.78 in the middle of the stem. The simple model of the motion was adequate to describe the UUCG base dynamics in both the loop and stem at 0 °C. There appeared to be no significant difference in the values of the order parameters for G·C and A·U pairs, consistent with the ^{13}C results for the IRE.

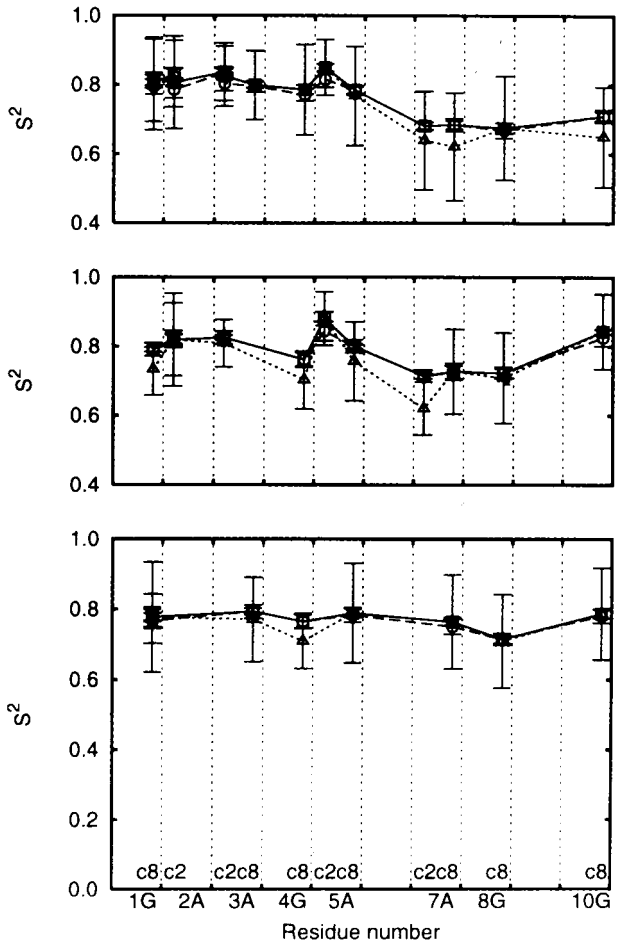

FIGURE 6: Order parameters (S^2) for each purine base in the IRE as a function of temperature (bottom, 20 °C; middle, 30 °C; and top, 37 °C) calculated with each model of the motion: (I) simple model, (○) model with R_{ex}, and (△) extended model. Errors were calculated from Monte Carlo simulation; errors in S^2 for the extended model are propagated from S_f^2 and S_s^2.

These results are similar to those of Gaudin et al. (*18*), who measured the ^{13}C T_1, $T_{1\rho}$, and NOE values of thymidine deoxyribose $^{13}C_{1'}$ in the middle of a DNA dodecamer. Over the temperature interval of 7−42 °C, the authors concluded that the amplitude of internal motion remained constant. Using the restricted rotation model to describe their data, they calculated a change in the sugar rotation around the glycosidic bond ($\Delta\chi$) of 28°. Borer et al. (*17*) used ^{13}C natural abundance to measure the NOE and T_1 values of short DNA oligonucleotides at 30 °C. Using the Lipari−Szabo model-independent formalism to describe the nucleotide dynamics, they found order parameters of the bases near 0.8, and lower values for the deoxyribose sugar ($S^2 = 0.6$). They observed that the 3′ base of one pentamer duplex had the lowest value of S^2 (∼0.5) which they attributed to fraying.

Loop. The structure of the IRE hairpin was solved at 20 °C, at the low salt concentration used for the dynamics measurements. Notable features of the loop structure included the two purine bases stacked on the 5′ side and the lack of NMR constraints describing the positions of two pyrimidines. Unfortunately, these dynamics data do not include information on 9U and 11C, the two pyrimidines that appear to be floppy. However, the temperature dependence of the dynamics of the stacked 7A and 8G, and the hydrogen-bonded 10G, shows that this loop structure is not rigidly maintained at higher temperatures at this low salt concentration.

At 20 °C, there is little difference between the order parameters or local correlation times of the purines in the loop and those in the stem. The exception may be 8G, which requires the extended model, with S_f^2 and S_s^2, to describe its relaxation. The NOEs that originally defined the stacking of 8G on 7A were weak, suggesting either that the distance between the two bases was long or that the stacking was unstable (*3*). In the models of the IRE generated from the NMR data, the 8G base was unstacked in one family of structures. These dynamics data suggest that 8G may be in motion at 20 °C. We note that in another IRE structure solved by NMR (*42*), again under low-salt conditions [10 mM NaCl, 10 mM sodium phosphate (pH 6.5), and 0.2 mM EDTA], the position of 8G was not constrained, and its glycosidic bond was described as syn. The loop structure is likely to be sensitive to ions and temperature, which may account for the differences.

The riboses of both 7A and 8G are best described as a mixture of C3′-endo and C2′-endo (*3*), whereas those of the stem are uniformly C3′-endo; the G10 ribose is C2′-endo. The heterogeneity in the ribose pucker of A7 and G8 does not correspond to a reduced order parameter for these two bases at 20 °C. However, the NOE ratio for 7A and 8G is larger than that of other bases, suggesting that these bases experience more motion on a fast time scale. Relaxation measurements of the riboses in the TAR RNA hairpin (*4*) and short DNA duplexes (*17*) showed that the sugars have smaller order parameters than their attached base; dynamics of the C1′ in a DNA duplex (*18*) resulted in estimates for τ_e of 10 ps. Assuming that similar ribose motions are present in the IRE, then one interpretation of the 7A and 8G base dynamics is that the time scale of the ribose repuckering is significantly faster than the base dynamics monitored here and thus the events appear uncorrelated. However, it is certainly not clear how the motions of the base and the sugar are related in either a stem or a loop.

As the temperature increases, there is evidence for more complex dynamic behavior of bases in the RNA loop. The dynamics of the loop and stem purine bases begin to show different patterns at 30 °C. Whereas at 20 °C the order parameters of all bases are similar, at 30 °C the order parameters of 7A and 8G in the loop become significantly reduced, and relaxation parameters for both bases are best fit by including both S_f^2 and S_s^2. Both 10G and 5A require significant exchange terms (for 5A C_8, the extended model of motion is required). This trend becomes more pronounced at 37 °C where all three loop purines have order parameters of approximately 0.65. 7A and 10G have large values of τ_s (0.6 and 1.5 ns, respectively), and 8G has a large exchange term (0.9 s^{-1}). It seems likely that the loop of the IRE has lost the stacking of 7A and 8G and the 10G−6C interaction that was described at 20 °C is not stable.

Models of the Motion. The order parameters for each base have also been used to estimate the standard deviation of rotation about the glycosidic bond, using the GAF model described by Bruschweiler and Wright (*36*) and applied to RNA bases by Akke et al. (*5*). In this model, the axis of rotation is defined by a vector coaxial to the glycosidic bond, and the base is allowed to rotate about this axis with a

Table 1: Relaxation Parameters of the IRE Hairpin Purines at 20 °C[a]

base	S^2	τ_e (ps)	R_{ex} (s^{-1})	S_f^2	τ_s (ns)	σ_χ (deg)
1G	0.77 ± 0.02	7 ± 8	0.32 ± 1.1			18
3A (C_8)	0.77 ± 0.13			0.80 ± 0.07	0.88 ± 1.1	18
4G	0.76 ± 0.02	25 ± 20				18
5A (C_8)	0.78 ± 0.02	20 ± 7	0.24 ± 1.1			18
7A (C_8)	0.75 ± 0.02	34 ± 7	0.54 ± 1.1			19
8G	0.71 ± 0.16			0.83 ± 0.08	0.14 ± 0.16	21
10G	0.78 ± 0.02	28 ± 8	0.24 ± 1.1			18

[a] τ_m = 3.65 ns. The choice of the model is determined by the magnitude of the residual of the fit and/or the realistic value of the parameters. The overall order parameter for the extended model is the product $S_f^2S_s^2$, and its error is propagated from the two order parameters. Errors in τ_e that would make the value negative have no meaning; the limiting value is 0. Errors in order parameters and correlation times are calculated from Monte Carlo simulation. No error is estimated for σ_χ.

Table 2: Relaxation Parameters of the IRE Hairpin Purines at 30 °C[a]

base	S^2	τ_e (ps)	R_{ex} (s^{-1})	S_f^2	τ_s (ns)	σ_χ (deg)
1G	0.79 ± 0.01	4 ± 8				18
2A (C_2)	0.82 ± 0.01	3 ± 20				15
2A (C_2)	0.82 ± 0.01	0 ± 5				15
3A (C_2)	0.82 ± 0.01	4 ± 10				15
4G	0.76 ± 0.02	41 ± 27				18
5A (C_2)	0.84 ± 0.03	0 ± 6	1.12 ± 1.2			14
5A (C_8)	0.76 ± 0.12			0.81 ± 0.06	1.0 ± 0.9	18
7A (C_2)	0.62 ± 0.09			0.77 ± 0.04	0.72 ± 0.2	25
7A (C_8)	0.73 ± 0.02	48 ± 26				20
8G	0.71 ± 0.15			0.81 ± 0.1	0.24 ± 0.2	21
10G	0.82 ± 0.02	26 ± 13	0.72 ± 1			16

[a] τ_m for the RNA is 2.94 ns.

Table 3: Relaxation Parameters of the IRE Hairpin Purines at 37 °C[a]

base	S^2	τ_e (ps)	R_{ex} (s^{-1})	S_f^2	τ_s (ns)	σ_χ (deg)
1G	0.79 ± 0.02	12 ± 6	0.32 ± 0.7			17
1G	0.81 ± 0.02	0 ± 5				17
2A (C_2)	0.82 ± 0.02	0 ± 5	0.8 ± 0.9			17
2A (C_2)	0.78 ± 0.02	21 ± 13	0.9 ± 0.9			17
3A (C_2)	0.83 ± 0.02	0 ± 8	0.11 ± 0.7			15
3A (C_2)	0.80 ± 0.02	6 ± 8	0.64 ± 0.81			15
3A (C_8)	0.8 ± 0.02	0 ± 6	0.144 ± 0.7			17
4G	0.77 ± 0.02	27 ± 8	0.44 ± 0.7			18
5A (C_2)	0.82 ± 0.02	0 ± 6	1.18 ± 1			16
5A (C_8)	0.77 ± 0.16			0.8 ± 0.1	0.7 ± 0.9	18
7A (C_2)	0.64 ± 0.18			0.74 ± 0.1	0.56 ± 0.33	23
7A (C_8)	0.62 ± 0.16			0.72 ± 0.1	0.61 ± 0.36	26
8G	0.67 ± 0.02	46 ± 6	0.91 ± 0.8			23
10G	0.65 ± 0.18			0.71 ± 0.1	1.54 ± 0.8	24

[a] τ_m for the RNA is 2.45 ns. Several bases have multiple resonances; each was analyzed separately.

Gaussian weighted distribution of angular displacement. This is a variant of the wobbling-in-a-cone model (*43*), and it translates the order parameters into a simple physical description of the motion of the plane of the base with respect to the fixed axis of the glycosidic bond.

The magnitude of the standard deviation (σ_χ) of the motion about the glycosidic torsion angle χ for bases in the IRE stem and loop derived from this model is quite large. At 20 °C, where the loop structure is well-defined, purine bases in the stem and in the loop have values of σ_χ between 18 and 19°; 8G in the loop, which has a lower order parameter, has a standard deviation of 21°. These values are similar to those obtained by Akke et al. (*5*) (σ_χ = 19−22°) from ^{15}N imino relaxation measurements for the UUCG tetraloop RNA, which was measured at 0 °C. In a related model of motion, Gaudin et al. (*18*) arrived at a value for $\Delta\chi$ of 28° for the deoxyribose excursions about the glycosidic bond in a DNA duplex.

The value of σ_χ for bases in the IRE stem does not change appreciably over the temperature range 20−37 °C, for it consistently varies from 15 to 18 °C. However, σ_χ values for purines in the loop reflect the order parameters becoming progressively smaller with increasing temperature, until at 37 °C, the loop purines have σ_χ values of 23−26°, which correspond to a 5−10° difference in σ_χ between loop and stem purines. It is not clear if this larger standard deviation represents a completely disordered structure or indicates larger excursions from the average structure.

The standard deviations in the angular displacements of the bases are here ascribed to motions about the glycosidic bond. However, it seems implausible that this is the isolated source of the flexibility of the base; the phosphodiester backbone and changes in the sugar pucker are both likely to contribute to motions of the base, especially in loop regions where there is conformational flexibility. Other more complex models have been used to describe the motions of

side chains in proteins and in lipids (*26*−*28*), but the application to a nucleic acid base will require knowledge of its sugar motions and its backbone dynamics. Meanwhile, a physical representation of the motions detected by the NMR relaxation experiments that can encompass all modes of motion may be best achieved through a molecular dynamics simulation of fully solvated RNA.

Molecular Simulations of RNA Structure and Dynamics

Several recent unrestrained molecular dynamics simulations of RNAs in solvent have been run for nanoseconds, allowing observation of the dynamics of the nucleotides. Of particular interest are three simulations with RNA hairpins: a 200 ps simulation of the GCAA tetraloop (*20*), several nanosecond simulations of the UUCG tetraloop (*21*), and a simulation of RNA duplexes (*22*); in addition, there is a 3 ns simulation of the $tRNA^{Asp}$ anticodon hairpin (*23*). The length of these simulations should allow the observation of the fast dynamic motions in the nucleotides that are reported by the NMR relaxation experiments.

The GCAA tetraloop simulation used Amber-OPLS force fields with sodium counterions and explicit waters, with electrostatics computed by Ewald sums (*20*). In a 200 ps simulation, there were transitions along the phosphate backbone involving the angles α, β, and γ (crankshaft transitions) observed after 15−35 ps in residues at the stem−loop junction; torsion angles of nucleotides in the stem fluctuate about the standard A-form values. Fluctuations about the glycosidic torsion angle (χ) appear to be relatively restricted; an estimate of the standard deviation from the polar plots (σ_χ) is 6−7°, with perhaps greater excursions for the 3′ terminal residue and the loop C. There was no sugar repuckering, although several riboses showed large fluctuations in the pseudorotation phase angle (120°). The author notes that there are correlated motions for the base atoms and the sugar−phosphate backbone, centered on the base and extending to three adjacent residues. The motions are divided, however, into those from the stem and those from the loop.

In the UUCG tetraloop simulations, AMBER 4.1 was used with sodium counterions, TIP3P water molecules, and Particle Mesh Ewald electrostatic treatment (*21*). The UUCG simulations showed very few incidences of crankshaft motions; in one conformation, 15 transitions were observed after 500 ps of molecular dynamics, while in another, two motions occurred after 100 ps. The standard deviations in the α, β, γ, and χ torsions were typically 9−20°, with larger fluctuations found at the second U of the loop. No ribose pucker changed over the course of the simulation, and the standard deviation in the pseudorotation angles was similar to fluctuations in other torsions. Similarly, during a 2 ns unrestrained MD simulation of an A-RNA duplex (*21*), no ribose repuckering was observed, although there were fluctuations in roll, tilt, and twist, which, together with base opening, may all be components of the dynamic motion appearing in the NMR experiments.

These molecular dynamics simulations of the RNAs did not report detailed trajectories for the motion about the different torsions. However, the length of the simulations puts them in a regime where some of the motions with picosecond correlation times that appear in the NMR dynamics analysis should be observed. In particular, the standard deviations reported for motion about the glycosidic bond in the simulations can be compared to the σ_χ derived from the NMR data. The simple GAF model calculated from the order parameters gives a σ_χ of ∼19° for motion about the glycosidic bond for those bases in a stem, which far exceeds the analogous value of about 8° found in the simulations. One simple explanation is that the GAF model is inadequate, since it effectively freezes out all other motions in the molecule and holds one degree of freedom responsible for the observed behavior. Alternatively, the simulations may be too short to sample larger amplitude motions that occur infrequently.

In the UUCG loop, the largest standard deviation about χ was at the second U in the loop (±60°); we would expect to see a similar value for 9U in the IRE loop even at 20 °C, while the other bases in the IRE loop should have relatively smaller amplitude excursions. The nucleotides in the GCAA loop are not as tightly constrained as the UUCG nucleotides, yet in that simulation, there were again no dramatic differences between the standard deviations of χ for stem and loop nucleotides. As noted, there was no ribose repuckering observed in the simulations; perhaps this is a consequence of the constrained structures of these RNA loops, for each ribose in the UUCG and GCAA RNAs is described experimentally by a single pucker. In contrast, the IRE loop riboses of 7A and 8G are best described as a mixture of C3′- and C2′-endo. It is important to know if there are correlated motions of bases and sugars that could contribute to the motion about χ; in fact, there needs to be a measurement of the time scale of ribose repuckering in various structural contexts, which can then be compared to simulation.

Future Directions

These experiments with the IRE are preliminary, for the picture of nucleotide motions must include the dynamics of the sugar and the phosphate backbone of the IRE. Measurement of ^{31}P T_1 and T_2 relaxation (*44*) as a function of temperature will undoubtedly show a difference between loop and duplex backbone motions. ^{13}C relaxation experiments for the ribose will require specific ^{13}C labeling to simplify the spin systems. In addition, we need to measure $\Delta\sigma$ of each ^{13}C, noting that the chemical shift tensor may be sensitive to local environment, such as stacking of aromatic bases, bound counterions, or hydrogen bonding of adjacent aromatic nitrogens.

The combination of NMR dynamics measurements and molecular dynamics simulations appears to offer the best approach for interpretation of the NMR results (*45*). The types of motions found in RNA structures, especially in regions of local conformational flexibility, may be understood only when all degrees of freedom of the phosphodiester backbone, sugar pucker, and glycosidic bond can be simultaneously sampled. For the IRE purines, the local correlation times observed in the NMR dynamics experiments are on the order of 3−40 ps which is in the range of the long MD simulations; when there are two time scales of motion, the longer correlation times range from 200 to 1500 ps, and while few if any of these motions would be adequately sampled in a one nanosecond simulation, longer simulations may be feasible.

ACKNOWLEDGMENT

We thank D. Jeremy Williams for many instructive discussions and W. Tom Stump for excellent technical assistance. Pulse sequences were obtained from the World Wide Web page of Prof. Lewis E. Kay, which is a wonderful community service.

SUPPORTING INFORMATION AVAILABLE

T_1, $T_{1\rho}$, and NOE data (3 pages). Ordering information is given on any current masthead page.

REFERENCES

1. Casey, J. L., Hentze, M. W., Koeller, D. M., Caughman, S. W., Roualt, T. A., Klausner, R. D., and Harford, J. B. (1988) *Science 240*, 924.
2. Gray, N. K., and Hentze, M. W. (1994) *EMBO J. 13*, 3882.
3. Laing, L. G., and Hall, K. B. (1996) *Biochemistry 35*, 13586.
4. King, G. C., Xi, Z., Michnicka, M. J., and Akratos, C. (1995) in *Stable Isotope Applications in Biomolecular Struct & Mechanisms*, pp 145−154, Los Alamos National Laboratory, Los Alamos, NM.
5. Akke, M., Fiala, R., Jiang, F., Patel, D., and Palmer, A. G. (1997) *RNA 3*, 702.
6. Kay, L. E., Torchia, D. A., and Bax, A. (1989) *Biochemistry 28*, 8972.
7. Nicholson, L. K., Yamazaki, T., Torchia, D., Grzeisiek, S., Bax, A., Stahl, S., Kaufman, J. D., Wingfield, P. T., Lam, P. Y. S., Jadhav, P. K., Hodge, C. N., Domaille, P. J., and Chang, C.-H. (1995) *Nat. Struct. Biol. 2*, 274.
8. Farrow, N. A., Zhang, O., Forman-Kay, J. D., and Kay, L. E. (1995) *Biochemistry 34*, 868.
9. Stone, M. J., Fairbrother, W. J., Palmer, A. G., III, Reizer, J., Saier, M. H., and Wright, P. E. (1992) *Biochemistry 31*, 4394.
10. Weaver, A. J., Kemple, M. D., and Prendergast, F. G. (1989) *Biochemistry 28*, 8624.
11. Wand, A. J., Urbauer, J. L., McEvoy, R. P., and Bieber, R. J. (1996) *Biochemistry 35*, 6116.
12. Lipari, G., and Szabo, A. (1982) *J. Am. Chem. Soc. 104*, 4546.
13. Lipari, G., and Szabo, A. (1982) *J. Am. Chem. Soc. 104*, 4559.
14. Peng, J. W., and Wagner, G. (1992) *J. Magn. Reson. 98*, 308.
15. Dayie, K. T., Wagner, G., and Lefevre, J. F. (1996) *Annu. Rev. Phys. Chem. 47*, 243.
16. Dellwo, M. J., and Wand, A. J. (1989) *J. Am. Chem. Soc. 111*, 4571.
17. Borer, P. N., LaPlante, S. R., Kumar, A., Zanatta, N., Martin, A., Hakkinen, A., and Levy, G. C. (1994) *Biochemistry 33*, 2441.
18. Gaudin, F., Paquet, F., Chanteloup, L., Beau, J.-M., Thuong, N. T., and Lancelot, G. (1995) *J. Biomol. NMR 5*, 49.
19. Williamson, J., and Boxer, S. (1989) *Biochemistry 28*, 2819.
20. Zichi, D. A. (1995) *J. Am. Chem. Soc. 117*, 295.
21. Miller, J. L., and Kollman, P. A. (1997) *J. Mol. Biol. 270*, 436.
22. Cheatham, T. E., and Kollman, P. A. (1997) *J. Am. Chem. Soc. 119*, 4805.
23. Auffinger, P., and Westhof, E. (1997) *J. Mol. Biol. 269*, 326.
24. Kemple, M. D., Yuan, P., Nollet, K. E., Fuchs, J. A., Silva, N., and Prendergast, F. G. (1994) *Biophys. J. 66*, 2111.
25. Daragon, V. A., and Mayo, K. H. (1998) *J. Biomol. NMR 130*, 329.
26. London, R. E., and Avitabile, J. (1978) *J. Am. Chem. Soc. 100*, 7159.
27. Lipari, G., and Szabo, A. (1980) *Biophys. J. 30*, 489.
28. Brainard, J. R., and Szabo, A. (1981) *Biochemistry 20*, 4618.
29. Nikonowicz, E. P., Sirr, A., Legault, P., Jucker, F. M., Baer, L. M., and Pardi, A. (1992) *Nucleic Acids Res. 20*, 4507.
30. Yamazaki, T., Muhandiram, R., and Kay, L. E. (1994) *J. Am. Chem. Soc. 116*, 8266.
31. Shaka, A. J., Barker, P. B., and Freeman, R. (1985) *J. Magn. Reson. 64*, 547.
32. States, D. J., Haberkorn, R. A., and Ruben, D. J. (1982) *J. Magn. Reson. 48*, 286.
33. Abragam, A. (1961) *Principles of nuclear magnetism*, Oxford University Press, Oxford, U.K.
34. Clore, G. M., Szabo, A., Bax, A., Kay, L. E., Driscoll, P. C., and Gronenborn, A. M. (1990) *J. Am. Chem. Soc. 112*, 4989.
35. Press, W. H., Teukolsky, S. A., Vetterling, W. T., and Flannery, B. P. (1988) *Numerical recipes in C*, 2nd ed., Cambridge University Press, Cambridge, U.K.
36. Bruschweiler, R., and Wright, P. E. (1994) *J. Am. Chem. Soc. 116*, 8426.
37. Roussel, A., and Cambillau, C. (1991) in *TURBO-FRODO in Silicon Graphics Partners Directory 86*, Silicon Graphics, Mountain View, CA.
38. Cavanagh, J., Fairbrother, W. J., Palmer, A. G., III, and Skelton, N. J. (1996) *Protein NMR Spectroscopy: Principles and practice*, Academic Press, San Diego.
39. Deverell, C., Morgan, R. E., and Strange, J. H. (1970) *Mol. Phys. 18*, 553.
40. Lane, A. N., and Lefevre, J.-F. (1994) *Methods Enzymol. 239*, 596.
41. Briki, F., Ramstein, J., Lavery, R., and Genest, D. (1991) *J. Am. Chem. Soc. 113*, 2490−2493.
42. Addess, K. J., Basilion, J. P., Klausner, R. D., Rouault, T. A., and Pardi, A. (1997) *J. Mol. Biol. 274*, 72.
43. Wittebort, R. J., and Szabo, A. (1978) *J. Chem. Phys. 69*, 1722.
44. Schweitzer, B. I., Gardner, K. H., and Tucker-Kellogg, G. (1995) *J. Biomol. NMR 6*, 180.
45. Palmer, A. G., III, and Case, D. A. (1992) *J. Am. Chem. Soc. 114*, 9059.

BI9805285